ELSEVIER

Chemical Engineering Journal 137 (2008) 653–663

Chemical Engineering Journal

www.elsevier.com/locate/cej

A micro-structured 5 kW complete fuel processor for iso-octane as hydrogen supply system for mobile auxiliary power units Part I. Development of autothermal reforming catalyst and reactor

Gunther Kolb [a,*], Tobias Baier [a], Jochen Schürer [a], David Tiemann [a], Athanassios Ziogas [a], Hermann Ehwald [b], Pierre Alphonse [c]

[a] *Institut für Mikrotechnik Mainz (IMM), Mainz, Germany*
[b] *Formerly Institute of Applied Chemistry (ACA, now Leibnitz Institute of Catalysis, LIKAT), Berlin, Germany*
[c] *CIRIMAT, University Toulouse III, Toulouse, Germany*

Received 8 January 2007; received in revised form 27 June 2007; accepted 30 June 2007

Abstract

A micro-structured autothermal reformer was developed for a fuel processing/fuel cell system running on iso-octane and designed for an electrical power output of 5 kW_{el}. The target application was an automotive auxiliary power unit (APU). The work covered both catalyst and reactor development. In fixed bed screening, nickel and rhodium were identified as the best candidates for autothermal reforming of gasoline. Under higher feed flow rates applied in microchannel testing, a catalyst formulation containing 1 wt.% Rh on alumina prepared by the sol–gel synthesis route proved to be stable at least in the medium term. This catalyst was introduced into the final prototype reactor designed to supply a 5 kW fuel cell, which was based upon micro-structured stainless steel foils. The reactor was optimised for equipartition of flows by numerical simulation. Testing in a pilot scale test rig, which was limited to a specified power equivalent of 3.5 kW_{el}, revealed more than 97% conversion of gasoline at 124 Ndm^3/min total flow-rate of reformate, which corresponded to a WHSV of 316.5 $Ndm^3/(h\ g_{cat})$.

Keywords: Microchannels; Micro-reactor; Octane reforming; Autothermal; Gasoline

1. Introduction

For mobile and portable applications of fuel cell technology, there is a need for compact hydrogen supply systems [1]. Fuel processors are a viable option for energy supply of fuel cells owing to the high energy density of liquid fuels such as alcohols and hydrocarbon mixtures. In case of gasoline and diesel, the existing distribution grid and availability on vehicles makes these fuels an attractive power source for mobile fuel cell based auxiliary power units (APU) on the short term. A fuel processor is composed of the reformer reactor itself and devices dedicated to remove the carbon monoxide out of the fuel, which is frequently performed by catalytic reactions such as water–gas shift and preferential oxidation [2]. Micro-structured reactors such as plate heat exchangers and ceramic or metallic monoliths bear a number of advantages compared to conventional technology such as fixed catalyst beds. Firstly, the pressure drop is significantly lowered owing to the laminar flow regime. Heat and mass transfer are improved in microchannels as well [1]. Specifically, the advantages of micro-structured catalyst coatings over fixed bed catalysts have been demonstrated for the autothermal reforming of iso-octane by Bae et al. [3] and for methanol steam reforming by Delsman et al. [4]. The work of Delsman et al. revealed, that micro-structured reformers and carbon monoxide clean-up reactors bear significant potential for reduction of reactor volume, insulation volume, catalyst mass and also total mass compared to conventional fixed bed technology even in the output power range of 5 kW_{el}.

At IMM, a complete fuel processor was developed and put into operation on a breadboard level, which was designed to supply a 5 kW fuel cell with purified reformate applying iso-octane as fuel. Iso-octane had been chosen as a model substance for

* Corresponding author.
E-mail address: Kolb@imm-mainz.de (G. Kolb).

1385-8947/$ – see front matter © 2007 Elsevier B.V. All rights reserved.
doi:10.1016/j.cej.2007.06.033

gasoline. Micro-structured plates coated with noble-metal-based catalysts were used to build the reactors either as monoliths or as cross-flow plate heat exchangers.

This paper deals with the development of the catalyst coating for the octane reformer reactor, the design of the reactor and single reactor tests at final scale.

2. Reaction system and feed composition

To gain hydrogen from liquid fuel, hydrocarbons are converted with steam in a reformer or with limited oxygen supply in a partial oxidizer unit, both reactions being heterogeneously catalysed [5,6]. Combining the endothermic steam reforming and exothermic partial oxidation of hydrocarbons results in the so-called autothermal reforming (ATR). In this process, the energy for the endothermic hydrocarbon steam reforming is produced by the exothermic partial oxidation of the hydrocarbons [7,8] thus resulting in an ideally thermally balanced reaction system.

Autothermal reforming applying air as oxygen source relates to the following basic formula for hydrocarbons:

$$3\text{–}CH_2\text{–} + O_2 + 4N_2 + H_2O \rightarrow 4H_2 + 3CO + 4N_2$$

$$\text{with} \quad \Delta H \approx 0$$

When the catalytic CO-clean-up is taken into consideration, which is usually to a large extent dominated by the water gas shift reaction, the overall stoichiometry of the fuel processor changes to

$$3\text{–}CH_2\text{–} + O_2 + 4N_2 + 4H_2O \rightarrow 7H_2 + 3CO_2 + 4N_2$$

In case, a low temperature PEM fuel cell is combined with the fuel processor, which is usually working around 85 °C and 3 bar, 20–25% of moisture in the fuel cell feed are required to prevent dry-out of the membrane. Thus, four molecules of water need to be added to the above formula and the following feed and reformate composition results:

$$3\text{–}CH_2\text{–} + O_2 + 4N_2 + 8H_2O \rightarrow 7H_2 + 3CO_2 + 4N_2 + 4H_2O$$

and specifically for iso-octane :

$$3C_8H_{18} + 8O_2 + 32N_2 + 64H_2O \rightarrow 56H_2 + 24CO_2 + 32N_2 + 32H_2O$$

which corresponds to a S/C ratio of 2.7 and about 22 vol.% of water in the fuel cell feed.

For the screening experiments described below, the S/C ratio was reduced to 2.27 corresponding to 15 vol.% water content of the reformate of. This leaves some space for water addition downstream the reformer, which may be required for temperature controlling purposes.

Iso-octane was applied as test fuel. Compared with straight chain hydrocarbons it is more easily cracked under reforming conditions, thus having a higher tendency towards coke formation. A reformer running stable on iso-octane is not expected to deactivate by coking from the other components of gasoline.

3. Catalysts

3.1. Catalyst development strategy

The reforming catalyst must be designed appropriately to ensure its stability in a high temperature oxidative steam atmosphere. Stabilized alpha-alumina, known by application as catalyst component in commercial steam reforming as well as stabilized zirconia are regarded as steam resistant carrier materials [9–12].

ATR catalyst development was focussing on supported VIIIb elements. The catalyst system and reaction conditions were chosen targeting at a high productivity towards hydrogen, suppression of coke formation and minimized methane selectivity.

The catalyst development was performed in two levels.

For primary screening purposes, catalyst samples were prepared as grains (0.5–0.7 mm) and tested in an integral fixed bed reactor described in Section 4.1.

For secondary screening, the best systems identified were coated onto micro-structured platelets and tested in the testing reactor described in Section 4.2.

From literature and former experience, a limited couple of catalytic systems were selected. Alumina as well as the zirconia carrier systems were chosen owing to their good stability under hydrothermally corrosive atmosphere. Active components tested were platinum, palladium, rhodium, ruthenium and nickel [13–17]. Lower stability was expected for the latter system.

3.2. Catalysts tested by screening experiments

The catalysts were prepared by incipient wetness impregnation with aqueous solution of the active component. Commercial zirconia and alumina tablets were ground and the 0.5–0.7 mm fractions were used as catalyst carriers. Zirconia samples had been delivered by MEL Chemicals, Manchester (EC0140E1/8). Alumina was purchased from Fluka (No. 06400). Table 1 provides an overview of the carrier materials applied and Table 2 summarizes the catalysts tested as fixed bed.

3.3. Catalysts tested as coatings in the micro-structured test reactor

Following the catalyst screening, Ni-alumina, Pt-alumina, Rh-alumina and Rh-zirconia coatings (see Table 3) were coated onto the micro-structured plates for incorporation into the test reactor.

Table 1
Carrier materials applied

	BET-surface area (m^2/g)	Pore diameter (Å)	Pore volume (ml/g)
Zirconia, MEL MeZr0404T1/8	10.2	336	0.085
Zirconia, MEL EC0140E1/8	87.1	99.0	0.215
Alumina, Fluka No. 06400	201	37.1	0.290

Table 2
Catalysts screened in fixed bed

Catalyst	Impregnation with	Carrier
7 wt.% Ni-ZrO_2	Ni $(NO_3)_2 \times 6H_2O$	ZrO_2; MEL, ECO140E1/8
7 wt.% Ni-Al_2O_3	Ni $(NO_3)_2 \times 6H_2O$	Al_2O_3; FLUKA, No 06400
1 wt.% Pd-ZrO_2	$PdCl_2 \times XH_2O$	ZrO_2; MEL, ECO140E1/8
1 wt.% Pt-ZrO_2	$Cl_6H_2Pt \times 6H_2O$	ZrO_2; MEL, MeTr0404T1/8
1 wt.% Ru-ZrO_2	$RuCl_3 \times XH_2O$	ZrO_2; MEL, ECO140E1/8
1 wt.% Rh-Al_2O_3	$RhCl_3 \times XH_2O$	Al_2O_3; FLUKA, No 06400
1 wt.% Rh-ZrO_2	$RhCl_3 \times XH_2O$	ZrO_2; MEL, ECO140E1/8

By sol–gel procedures based on alkoxide hydrolysis, alumina-based and zirconia-based catalyst layers were synthesized. Zirconia layers were deposited on alumina-pre-coated platelets.

3.3.1. Synthesis of sols

The synthesis of the alumina sols, precursors of the catalyst layers, was based on the method originally proposed by Yoldas [18]. The first step of the process was the hydrolysis of aluminum trisec-butoxide, $Al(OC_4H_9)_3$) at 85 °C in a large excess of water ($H_2O/Al = 100$) containing the required amount of the rhodium precursor ($RhCl_3$,xH_2O). This gave an aluminum hydroxide slurry that was subsequently peptized to a clear sol by addition of nitric acid ($HNO_3/Al = 0.07$). After peptization (24 h), the sols were concentrated by heating at 85 °C, until they became thixotropic [19].

3.3.2. Coating of the metallic substrates

The first step was the surface treatment of the stainless steel in order to ensure an optimal adhesion between the layer and the substrate. In this operation, the plates were immersed in an alkaline cleaner (TurcoTM 4181) at 75 °C for 30 min. Then they were rinsed with water in an ultrasonic bath. Finally, they were dried and heated in air at 500 °C for 2 h.

The coating on micro-structured metallic substrates was performed by tape casting, in such a way that the sol remained only inside the microchannels. After coating, the plates were dried overnight at room temperature. The final step was a calcination in air, at a temperature in the range from 500 to 800 °C, for 2 h.

The maximum thickness obtained from concentrated sols was 2.4 μ with a standard deviation of 0.35 μm.

Thin films have been coated on PTFE substrates for the microstructural characterizations. After drying at room temperature, films could be easily separated from the substrate. These xerogels were reduced to powders by grinding.

Table 3
Catalysts tested as coatings in the microchannels

Platelet coating composition	Catalyst mass per platelet pair (mg)
Al_2O_3	35.4 ± 0.2
0.1 wt.% Rh/Al_2O_3	19.3 ± 0.2
0.5 wt.% Rh/Al_2O_3	43.7 ± 0.2
7 wt.% Ni/Al_2O_3	54.9 ± 0.2
1 wt.% Rh/Al_2O_3	46.6 ± 0.2
2 wt.% Rh/Al_2O_3	49.7 ± 0.2

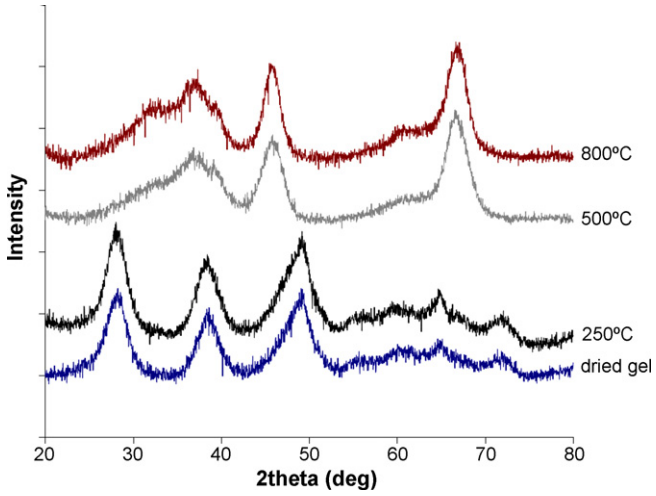

Fig. 1. Effect of heating temperature on powder XRD patterns of 2 wt.% Rh xerogels (Seifert 3003TT θ–θ diffractometer in the Bragg–Brentano geometry, using filtered Cu K α−radiation and a graphite secondary-beam monochromator).

3.3.3. Catalyst characterization

XRD and TEM show that xerogels were essentially composed of nanosized crystals of boehmite (AlOOH). On heating, the boehmite structure was maintained up to 400 °C, then progressive transformation in transition alumina (γ-alumina) occurred (Fig. 1).

EDX analysis indicated that Rh was uniformly distributed in alumina carrier. It was impossible to detect the presence of Rh in the X-ray diffraction patterns even for the 2 wt.% Rh-catalysts.

Nitrogen adsorption experiments revealed that whatever the heating temperature, the xerogels were essentially mesoporous. The average pore diameter increased from 3 nm at 400 °C to 8 nm at 800 °C. The porous volume, about 0.3 cm^3/g, did not change much with temperature. The specific surface area reached a maximum at 450 °C. Above this temperature, it decreased almost linearly (from 400 m^2/g at 500 °C to 150 m^2/g at 800 °C). The addition of Rh in alumina slightly increased the specific surface area and decreased the average pore diameter (Fig. 2).

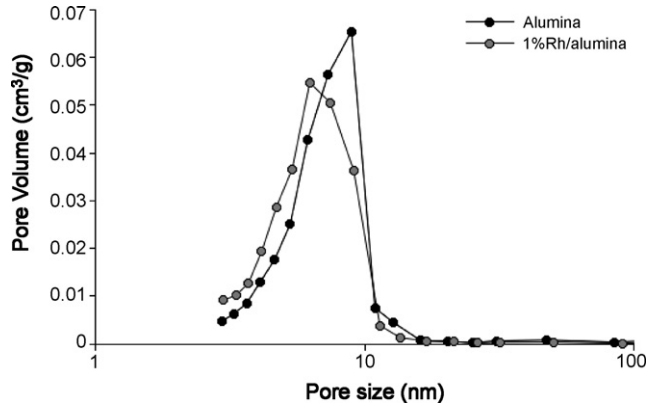

Fig. 2. Comparison between pore size distributions (PSD) of alumina and 1 wt.% Rh/alumina catalysts heated at 800 °C in air for 10 h (PSD computed – using BJH method – from N_2 desorption isotherms at 77 K recorded with a Micromeritics ASAP 2010M).

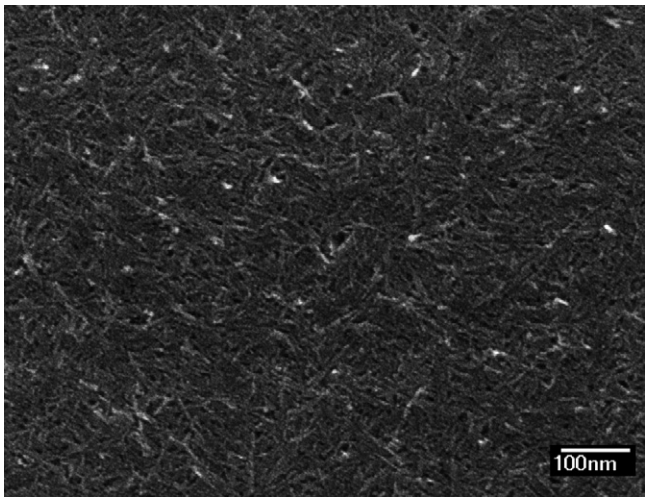

Fig. 3. Scanning electron microscopy (SEM) of 1 wt.% Rh/alumina catalyst heated at 500 °C in air (JEOL JSM 6700, 5 kV).

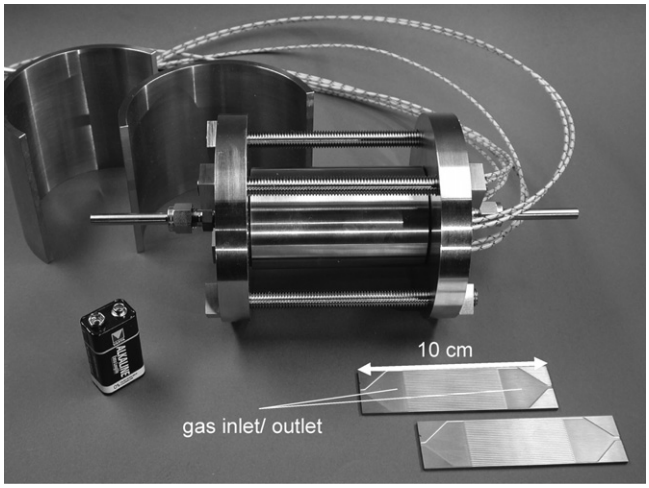

Fig. 4. The testing reactor for developed for the screening of reformer catalyst coatings.

The SEM images of the coatings on micro-structured plates showed that the catalyst layer filled quite well the roughness of the steel substrate. The large porosity created by the fibrous structure of the catalyst layer was also clearly visible (Fig. 3).

3.4. Catalyst applied for the final 5 kW reformer

Coating of the plates for the 5 kW reformer (200 plates) was performed with a 1 wt.% Rh-alumina catalyst. In both cases, the average thickness of the coating ranged between 2 μm and 3 μm. The coating procedure was identical to the procedure described in Section 4.2.

The total amount of catalyst incorporated into the reactor was 19.8 g, which corresponds to 0.2 g of the active Rh species.

4. Testing devices

4.1. Testing reactor for fixed bed testing

The ATR experiments were carried out at 2 bar pressure in a quartz glass annular gap reactor consisting of three concentric tubes. The catalyst (0.5–0.7 mm particle size) was filled in the void volume between the 12 mm diameter outer and the 9 mm diameter middle tubes (cross section of the annular gap equals 32 mm^2, height of the catalysts bed usually 15–20 mm). The educt mixture was preheated in the void volume above the catalyst bed, and the product mixture was taken on top of the middle tube. Within the inner tube, a thermocouple was positioned. The reactor is described in detail in [20,21]

4.2. Development of the testing reactor for catalyst coatings

A testing reactor was designed for the development of the catalyst coatings. It was designed to take up two micro-structured platelets. Because catalyst screening was the target application of the reactor, the platelets needed to be exchangeable. The reactor, which is shown in Fig. 4, was composed of a core taking up the platelet pair, which was heated by electrical heating cartridges (see Fig. 5). Two flanges with a conical gap (see Fig. 6) compressed the platelets face to face and also the inlet and outlet tubes against the platelets. Thus, a metallic sealing concept was realised, which sealed the process gas flow from the reactor body. This was necessary, because the reactor body, flanges and screws were fabricated from nickel based alloy (2.4650 German code containing 20 wt.% Cr, 20 wt.% Co, 5 wt.% Mo and 2 wt.% Ti, balance Ni). Thus, suspicion arose that enhanced coke formation was to be expected at the surface of the nickel-based alloy. The platelets themselves along with the in- and outlet tubes were fabricated from nickel-free stainless steel (1.4742 German code containing 18 wt.% Cr, 1 wt.% Al, 1 wt.% Si, 1 Wt.% Mn, balance Fe). They were designed for a feed flow rate of 100 Ncm^3/min at a pressure drop of 8 mbar. Each platelet carried 40 microchannels with a length of 50 mm at a channel height of 300 μm and a channel width of 400 μm. Inlet and outlet sections had identical geometry. The channels were introduced by wet chemical etching into the platelets. As a second sealing concept, graphite gaskets were incorporated into the flanges of the reactor, to ensure sealing to the environment. Because the gaskets were protected against the environmental oxygen exposure in the

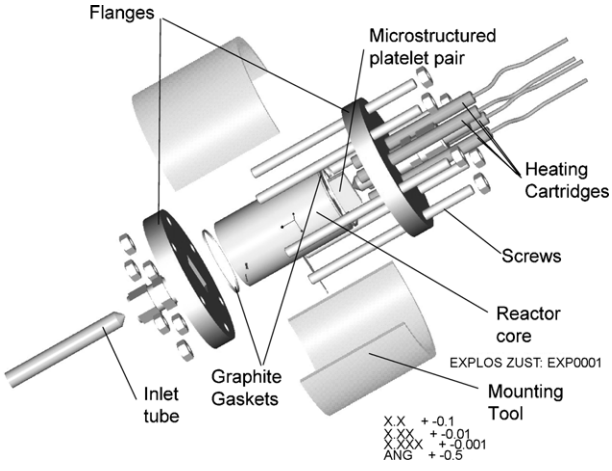

Fig. 5. Explosion view of the testing reactor.

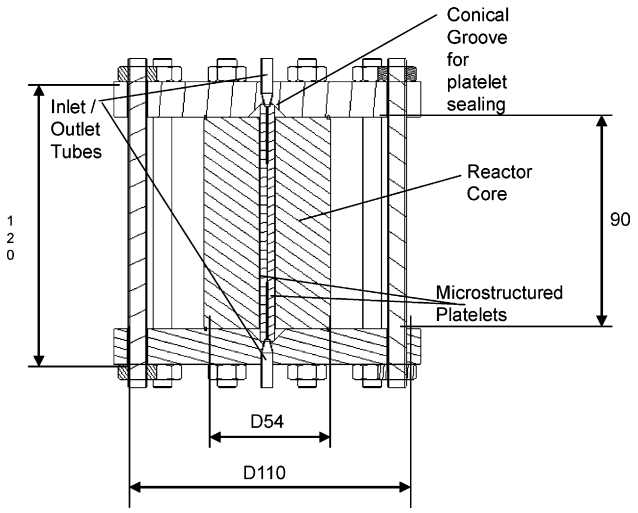

Fig. 6. Cross-sectional view of the testing reactor.

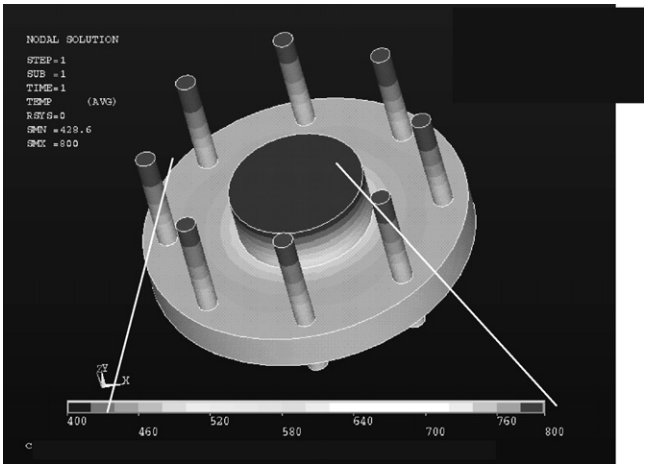

Fig. 7. Simulation of the temperature distribution in the testing reactor during operation; a convection coefficient of 15 W/m^2 and a heat conductivity of 15 W/(mK) were assumed for the calculations.

groves of the flanges, their lifetime proved to exceed 100 h in most cases during practical operation of the reactor. The screws attaching the flanges against the reactor body were thermally decoupled from it, thus minimising their operating temperature. Numerical simulations performed with ProEngineer software at the 3D-CAD model of the reactor revealed a temperature well below 500 °C for the screws in case the reactor core temperature was set to 800 °C (see Fig. 7).

The reactor was designed for a maximum operating temperature of 800 °C and a maximum operating pressure of 4 bar. Leak–tightness of the reactor was proven prior to first operation at 700 °C and a pressure of even 10 bar. The reactor proved good operability during 3100 h of experimental operation, in which 60 catalysts were tested and two long-term experiments of 100 h operation were performed.

5. Catalyst evaluation

5.1. Experimental

The feed composition described in Section 2 was applied for the catalyst screening experiments performed at LIKAT (former ACA institute). Table 4 provides the flow rates and feed composition applied along with the maximum achievable hydrogen productivity.

The reactor and all tubing carrying condensable components had been accommodated in an air thermostat keeping the temperature of the system periphery at 150 °C (see Fig. 8). The gas flows were adjusted and monitored by mass flow controllers. A gas chromatograph HP5890 (on line) was used for analysing the hydrocarbons in the product mixtures. A Baltzers quadrupole mass spectrometer (MS) type QMS 200 provided the on line data of H_2, O_2, H_2O, CO, CO_2 and He, which was fed with sample by heated mass-flow and back-pressure controlling valves. For the analysis of CO by MS a 1:4 molar oxygen/helium mixture was applied instead of air.

During the initial fixed bed experiments, catalytic activities were determined at a total pressure of 2 bar in the integral reactor described above with 500 mg ground catalyst (0.5–0.7 mm).

5.2. Results from catalyst screening

Fig. 9 shows the results of screening tests of several ground catalysts at 750 °C and a feed rate of 5 ml/h liquid i-octane as obtained in the integral reactor. The catalysts can be divided into two groups according to their basic performance. With the first group – 7 wt.% Ni/ZrO_2, 7 wt.% Ni/Al_2O_3, 1 wt.% Rh/ZrO_2 and 1 wt.% Rh/Al_2O_3 catalysts – the highest hydrogen productivities were obtained. The second group – 1 wt.% Pd/ZrO_2, 1 wt.% Ru/ZrO_2 and 1 wt.% Pt/ZrO_2 catalysts – produced significantly less hydrogen and, as shown in Fig. 10, more methane and hydrocarbon by-products were found compared with the first group. Therefore, further experiments applying coated platelets

Table 4
Feed rates and corresponding maximum achievable hydrogen productivity

i-Octane (ml_{liquid}/h)	H_2O (ml_{liquid}/h)	O_2 (l_{gas}/h)	He (l_{gas}/h)	C:O:H_2O	H_2 achievable[a]
Screening experiments (mmol/h)					
5	10	2	8	1:0.68:2.26	
30.6	555.6	167	667		472
Micro-reactor experiments (mmol/h)					
10	20	4	16		
61.3	1,111.1	484.3	1,937.4		944

[a] H_2 molar flow achievable is calculated assuming a CO/CO_2 ratio of 1.

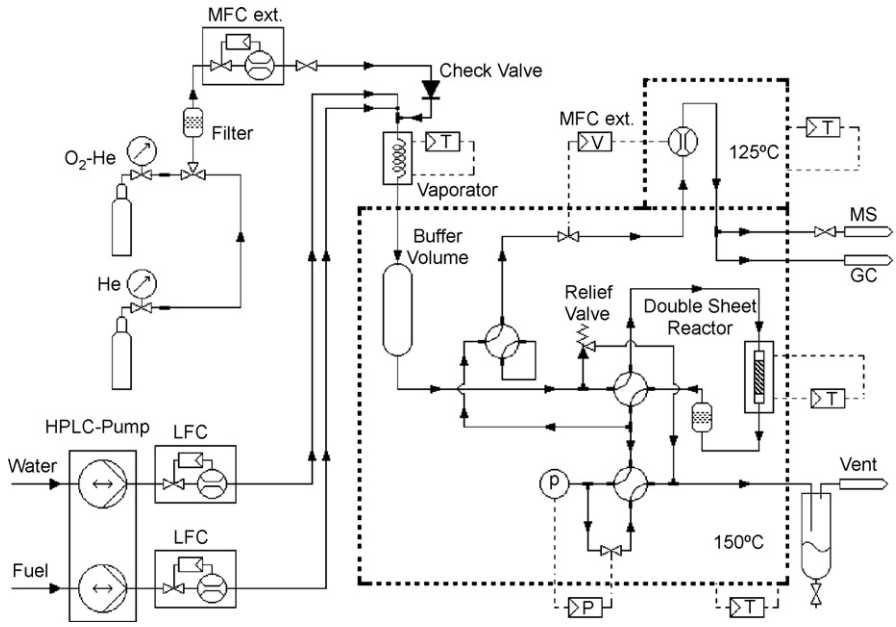

Fig. 8. Flow scheme of the test rig applied for catalyst screening; the part of the equipment, which was incorporated into the air thermostat is surrounded by the dotted line.

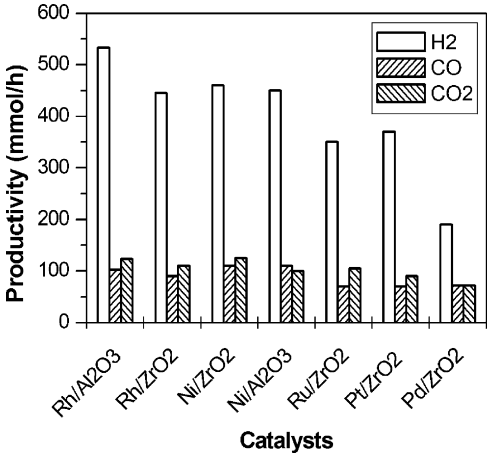

Fig. 9. Comparison of species molar flow for hydrogen and carbon during autothermal reforming over different types of catalysts—fixed bed screening.

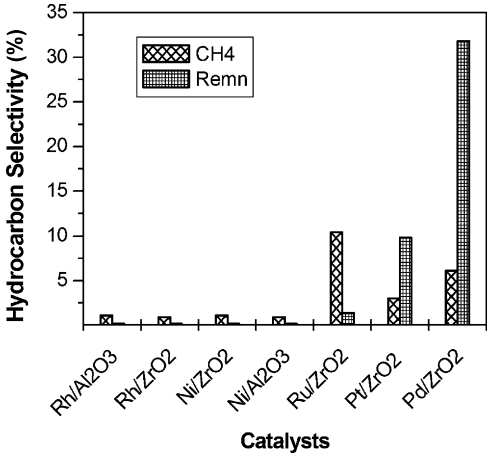

Fig. 10. Comparison of hydrocarbon formation during autothermal reforming over different types of catalysts—fixed bed screening.

were performed exclusively with catalyst coatings based upon formulations similar to the first group.

Experiments applying coated platelets, in contrast to the experiments performed in fixed bed, provided satisfactory results only with 1 wt.% and 2 wt.% Rh/Al_2O_3. The 7 wt.% Ni/Al_2O_3 coating was as inactive as the alumina carrier (see Fig. 11). This may be at least partially attributed to the significantly higher weight hourly space velocity applied for these experiments compared to fixed bed testing. The flow rate was two times higher in the microchannel reactor, but the mass of catalyst coatings amounted to merely 50 mg compared to 500 mg for the fixed bed.

As shown in Fig. 12, platelets coated with catalysts consisting of 0.5 wt.%, 1 wt.% or 2 wt.% Rh on Al_2O_3 provided high i-octane conversion and high selectivities towards hydrogen.

Thus, the catalytic system Rh/Al_2O_3 with 1–2 wt.% Rh/Al_2O_3 was regarded as the most convenient coating formulation for autothermal octane reforming in microchannels.

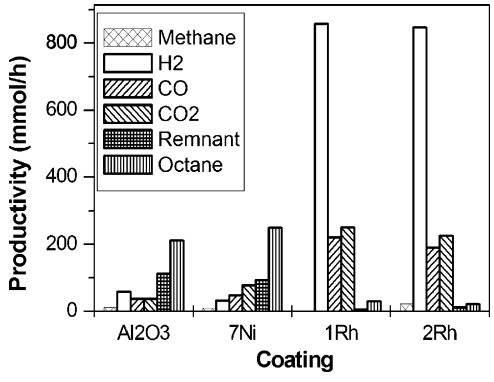

Fig. 11. Comparison of species molar flow for hydrogen, carbon oxides, methane and remaining hydrocarbons during autothermal reforming over different types of catalyst coatings in microchannels.

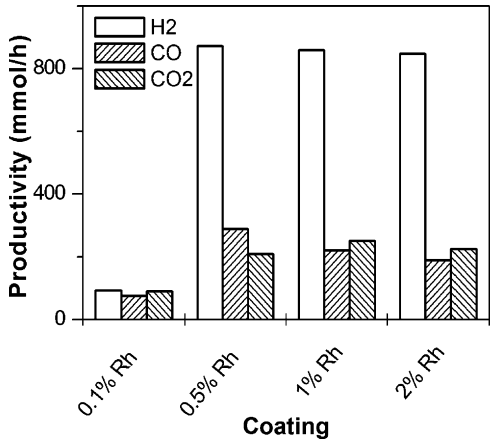

Fig. 12. Comparison of species molar flow for hydrogen and carbon oxides during autothermal reforming over different types of catalyst coatings in microchannels—effect of Rh loading.

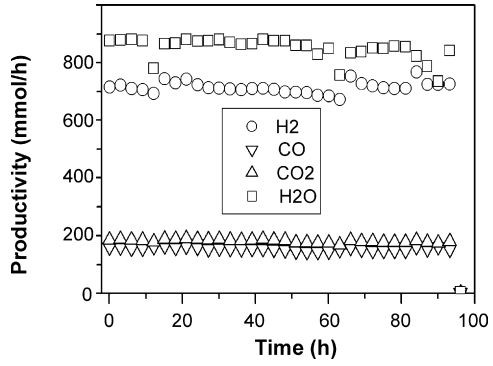

Fig. 13. Long-term stability test of the 1 wt.% Rh catalyst coating; molar flows of carbon oxides, steam and water as determined in the testing reactor.

The long time stability (Figs. 13–15) of platelets coated with 1 wt.% Rh/Al_2O_3 was measured with 10 ml i-octane/h. The activity declined only slowly during 100 h, returning after short oxidation periods (14 h, 64 h and 84 h) to the initial level. These oxidation periods were caused by short i-octane feed stops because of difficulties with the HPLC pump used. Owing to the observed coke formation over the catalyst, it was concluded to

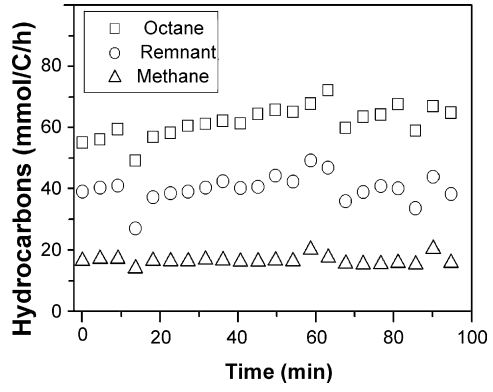

Fig. 14. Long-term stability test of the 1 wt.% Rh catalyst coating; molar flows of hydrocarbons as determined in the testing reactor.

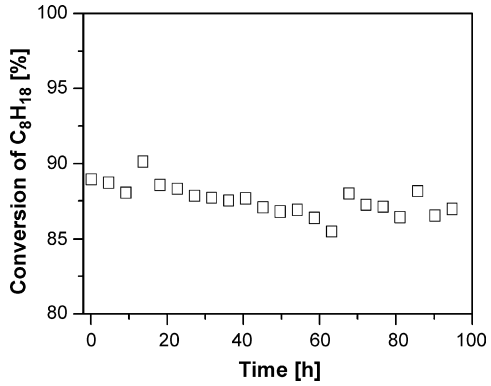

Fig. 15. Long-term stability test of the 1 wt.% Rh catalyst coating; iso-octane conversion as determined in the testing reactor.

run the final ATR reactor of the fuel processor at S/C ratio of 3.3 to suppress coke formation.

6. Realization and testing of the 5 kW autothermal reformer

6.1. Development of the 5 kW autothermal reformer reactor

The autothermal reformer, which was developed at IMM is shown in Fig. 16. It is composed of 200 micro-structured metal foils of 400 μm thickness carrying a total of 25,000 channels each 400 μm wide and 250 μm deep. This corresponds to a channel density of 2520 channels/in.^{2} and a total surface area of 2.6 m^2. The reactor has a width and height of 80 mm at a total length of 250 mm. It has a monolithic design. The reactor was pre-heated electrically to 120 °C by heating cartridges which were incorporated into two plates on top and at the bottom of the reactor (not shown in Fig. 16). Most of the pre-heating up to operating temperature was performed by hot air and steam respectively during start-up.

To check for the equipartition of the gas flow through all channels of the stack, numerical simulations were performed. For the diffuser section, a fine grid was necessary in order to resolve the flow field. In total, the number of elements used was approximately 840,000. The simulations were carried out

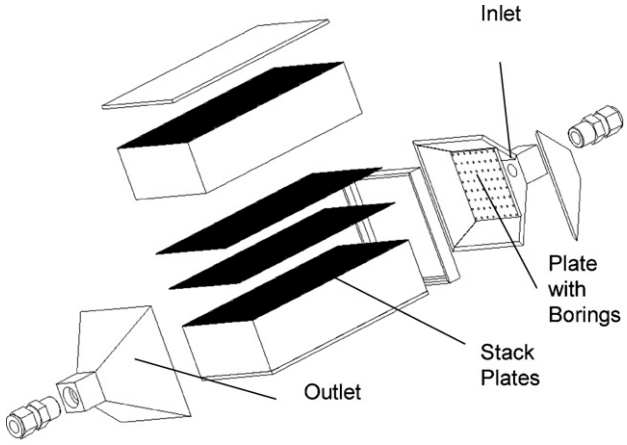

Fig. 16. Explosion view of the ATR reactor.

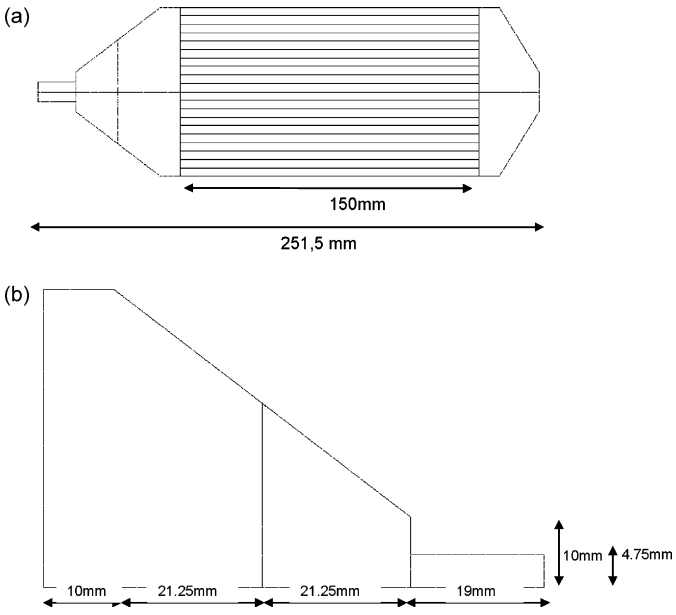

Fig. 17. (a) Geometry applied for calculations. (b) Cross-sectional view of the inlet diffuser.

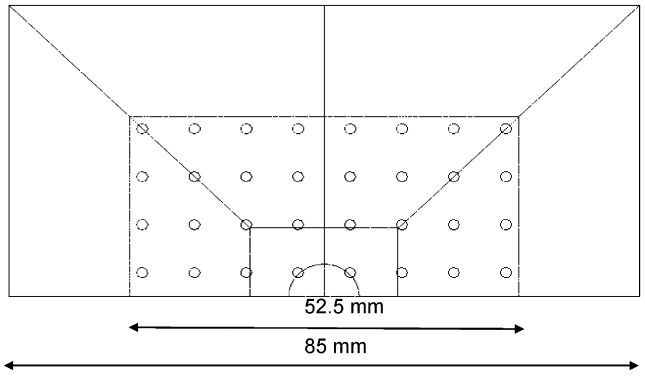

Fig. 18. Geometry A of the perforated plate.

using the commercially available finite volume solver CFX 5.6. Due to the large Reynolds number in the inlet section, a standard k-epsilon turbulence model was used. Fig. 17a shows the basic geometry of the system, the hatched area indicates the microchannels. This area was simulated by a matrix of 10 × 10 bigger channels (2 mm × 2 mm) which carried a porous medium that had a pressure drop identical to the microchannels. This way the time demand of the calculations was significantly reduced and results were still of satisfactory precision. Fig. 17b shows a cross section of the inlet diffuser. For the sake of reducing the time demand of the calculations, only a quarter of the geometry was simulated owing to its symmetry. Calculations assuming free flow of the feed into the reactor revealed a maximum of 16% deviation from the average velocity in the core of the gas jet. Therefore, a perforated plate was introduced in the middle of the inlet diffuser (indicated as a dashed line in Fig. 17a) to achieve equipartition. Fig. 18 shows geometry A out of numerous designs, which were checked by simulations. The radius of the holes amounts to 7 mm, the distance between the holes to 7 mm as well. Fig. 19 illustrates the effect of the perforated plate on the velocity field; the gas jet entering the inlet diffuser in the centre is slowed down and distributed. Fig. 20 shows the velocity distribution with the perforated plate of geometry A. As seen from the plot in Fig. 20, the deviation from the average value ranges around 1% from the centre of the corners of the reactor, which is regarded as satisfactory for the applica-

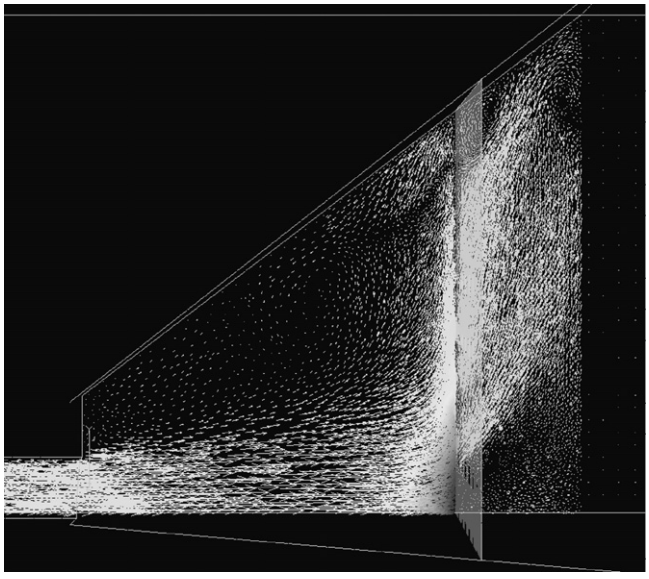

Fig. 19. Effect of the perforated plate on the velocity field.

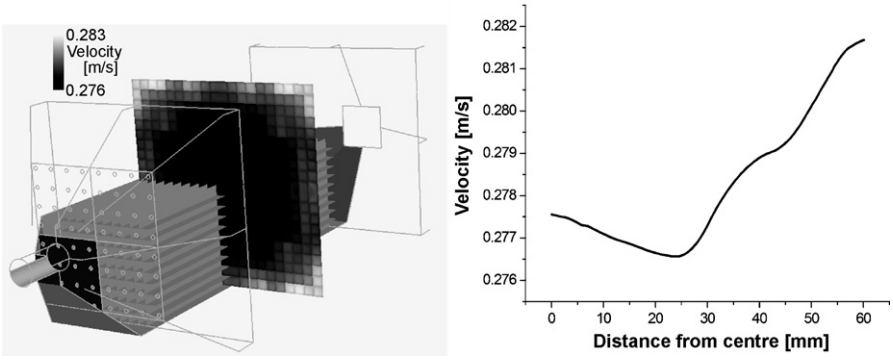

Fig. 20. Left: whole geometry with a perforated plate of geometry A and velocity distribution in the channels. Dimensions as specified in Fig. 17. Right: averaged velocity distribution along a diagonal from the centre to one of the corners of the reactor.

Fig. 21. Pressure distribution over the reactor. Dimensions as specified in Fig. 19.

tion. Fig. 21 shows the pressure distribution over the reactor. The pressure drop in the microchannels was calculated to be 11 mbar, the overall pressure drop of the reactor amounted to 14 mbar. A pressure peak of 20 mbar above reactor outlet pressure was calculated owing to impact pressure before the centre of the perforated plate.

A 1 wt.% Rh on alumina sol carrier catalyst (see above) was coated onto the micro-structured plates, which were prepared from stainless steel foils by wet chemical etching with iron (III) chloride, sealed by laser welding and put into a stainless steel housing to assure mechanical stability at the maximum operating temperature of 800 °C and the maximum operating pressure of 4 bar.

6.2. Testing of the 5 kW autothermal reformer

6.2.1. Experimental

Below function of the test rig will be briefly explained, which was used to test the final reactor. Steam was generated externally by a conventional 8 kW evaporator and superheated to 650 °C in a 3 kW micro-structured gas heater and then introduced into the reactor inlet, whereas iso-octane vapour, produced by a second, 3 kW evaporator was introduced into the reactor directly at the inlet diffuser. This arrangement avoided the occurrence of homogeneous reactions in the equipment upstream the reactor itself (i.e. in the gas heater). Both evaporators were fed by gear pumps. The oxygen supply, which was performed separately as well as nitrogen for balancing the synthetic air feed and for system purging was regulated by conventional thermal mass flow meters (Bronkhorst). The steam/air mixture could be by-passed around the reactor. A pneumatically driven pressure control valve (Kemmer) regulated the system pressure. Water-cooled condensers reduced the temperature of the reactor product flow and removed the steam before it entered the exhaust system.

Four temperatures at the reactor body were monitored during the experiments. One temperature was measured at the reactor inlet (inside the diffuser upstream the perforated plate), two temperatures after 7.5 mm and 27.5 mm, respectively in the centre of the plate stack. Finally, the temperature of the product gases was determined at the outlet diffuser of the reactor.

The concentration of the various species present in the reactor off-gas was detected by an online micro gas chromatograph (Varian CP-4900 Micro-GC). It consisted of four different channels each with a separate TCD detector and oven. Channel 1 had a 10 m long molsieve column which could separate O_2, N_2 and CO, channel 2 had a similar column to separate H_2 and CH_4, channel 3 had a Porapak U column to separate CO_2, H_2O and species up to butane. Finally, Channel 4 was equipped with a 6 m 5 CB column for alkane separation. All channels used helium as carrier gas with the exception of Channel 2 which used N_2 as carrier gas and column pressure was in all cases 150 kPa. Each analysis lasted for 1 min while it was possible to have an analysis cycle of ca. 1.5 min. However, its drawback was, that only a water content of less than 15 vol.% could be tolerated by the instrument. Thus, all water was removed out of the gas flows before entering the GC by a tube filled with molecular sieve and results of analysis are reported on a dry basis (d.b.). In order to gain information about the degree of octane conversion, a separate analysis method was developed, which comprised of additional sampling of product gas, which was washed by acetonitrile to selectively absorb the octane. The analysis was then performed subsequently at an off-line GC–MS system. This way, the degree of conversion could be determined with a precision of 3% absolute.

6.2.2. Results

The reactor was operated at a maximum WHSV of 316.5 $Ndm^3/(h\ g_{cat})$. The electrical heating of the reactor was used for pre-heating it to a temperature above 100 °C to avoid condensation. Most of the pre-heating of the reactor was performed applying a mixture of nitrogen and steam as heat carrier, which was fed directly into the reaction channels. Table 5 summarises experimental conditions and measurements as determined for the reactor under different steam to carbon ratios. The reactor was operated under autothermal conditions for a total duration of more than 3 h during this test run. The steam to carbon ratio (S/C) of the feed was continuously decreased from 5.1 to 3.3 by increasing the iso-octane and oxygen feed rate while keeping the nitrogen and steam flow rate constant. The oxygen to carbon ratio (O/C) was maintained constant at 0.65 and the WHSV was set to values around

Table 5
Experimental settings, product composition and temperatures as determined for the 5 kW ATR reactor at different S/C-ratios

	System pressure (bar)		
	3	3	3
S/C	5.1	3.9	3.3
O/C	0.65	0.64	0.64
Feed flow rates			
$F(N_2)$ (Ndm^3/min)	25.3	25.3	25.3
$F(O_2)$ (Ndm^3/min)	2.5	3.2	3.9
$F(C_8H_{16})$ (Ndm^3/min)	0.96	1.26	1.51
$F(H_2O)$ (Ndm^3/min)	39.6	39.6	39.6
Total feed flow rate (Ndm^3/min)	68.3	69.3	70.3
WHSV ($Ndm^3/(h\ g_{cat})$)	207.1	210.1	213.0
Product composition (d.b.)			
$C(H_2)$ (vol.%)	29.8	32.9	35.4
$C(CH_4)$ (vol.%)	0.2	0.4	0.7
$C(N_2)$ (vol.%)	54.2	48.4	44.2
C(CO) (vol.%)	3.3	4.4	5.7
$C(CO_2)$ (vol.%)	10.1	11.2	11.6
$C(O_2)$ (vol.%)	0.0	0.0	0.0
T (inlet) (°C)	720	720	720
T (X = 7.5 cm) (°C)	725	730	730
T (X = 27.5 cm) (°C)	710	710	710
T (outlet) (°C)	700	700	700

Table 6
Experimental settings, product composition and temperatures as determined for the 5 kW ATR reactor at different O/C-ratio, S/C ratio and reactor inlet temperature

	System pressure (bar)		
	3	3	3
S/C	3.3	3.6	3.6
O/C	0.52	0.59	0.59
Feed flow rates			
$F(N_2)$ (Ndm^3/min)	25.25	25.25	25.25
$F(O_2)$ (Ndm^3/min)	5.6	5.8	5.8
$F(C_8H_{16})$ (Ndm^3/min)	2.67	2.46	2.46
$F(H_2O)$ (Ndm^3/min)	70.9	70.9	70.9
Total feed flow rate (Ndm^3/min)	104.5	104.4	104.4
WHSV (Ndm^3/(h g_{cat}))	316.5	316.5	316.5
Product composition (d.b.)			
$C(H_2)$ (vol.%)	42.4	41.9	42.2
$C(CH_4)$ (vol.%)	2.6	2.7	2.8
$C(N_2)$ (vol.%)	34.3	34.5	36.6
C(CO) (vol.%)	7.7	7.4	6.7
$C(CO_2)$ (vol.%)	13.6	13.9	14.1
$C(O_2)$ (vol.%)	0.0	0.0	0.0
T (inlet) (°C)	725	725	600
T (X = 7.5 mm) (°C)	730	750	725
T (X = 27.5 mm) (°C)	700	725	690
T (outlet) (°C)	680	700	675

210 Ndm^3/(h g_{cat}). The results of the GC analysis provided in Table 5 revealed an increasing hydrogen content of the gaseous products as expected. Analysis of the liquid product revealed only negligible content of iso-octane indicating more than 97% conversion of the hydrocarbon feed. The temperature profile inside the reactor was relatively flat under the conditions described in Table 5 owing to the rather low iso-octane feed rate.

Table 6 shows results from experiments as performed at higher WHSV of 316.5 Ndm^3/(h g_{cat}). These experiments were performed at lower O/C ratio of the feed. The gas composition, which is provided in Table 6, agrees well with the expected result from stoichiometry, when equilibrium of the water–gas shift reaction is assumed at a temperature of 725 °C, which corresponds to the hot spot temperature of the reactor. The methane formation was relatively high for a temperature of 725 °C and exceeded the thermodynamic equilibrium. When decreasing the reactor inlet temperature from 725 to 600 °C lowered the hot spot temperature of the reactor, and the dry reformate composition changed as expected into the direction of the equilibrium of the water–gas shift reaction. However, owing to the relatively small temperature drop of 25 K (see Table 6) along the reactor axis, the shift of carbon oxide content and the increase of methane in the reformate was only moderate.

Changing the system pressure from 3 bar to both 2.5 bar and to 4.0 bar did neither affect the reactor performance nor the reformate composition. When stopping the i-octane, oxygen and steam flow to the reactor and purging with nitrogen, it emptied very quickly and within less than 3 min no hydrogen could be detected any more documenting the narrow residence time distribution in the reactor and the test rig.

The content of light C_2 and C_3 alkanes in the reformate was very low, never exceeding 0.02 vol.%.

The efficiency of the reformer was calculated according to Severin et al. [22]:

$$\eta = \frac{(\dot{n}_{H_2} + \dot{n}_{CO})\mathrm{LHV}_{H_2}}{\dot{n}_{C_8H_{18}}\mathrm{LHV}_{C_8H_{18}}}$$

LHV represents the lower heating value. At S/C 3.6 and O/C 0.59 an efficiency of 78.3% was achieved, at S/C 3.3 and O/C 0.52 even 79.8%.

Severin et al. found values around 80% at O/C 0.6 and even 85% at O/C 0.52 for the efficiency of their ATR reactor, which was based on a ceramic monolith and designed for a power output of 3 kW_{el}. The dry gas hydrogen content of the reformate was 38 vol.% at O/C ratio 0.6 and S/C ratio 2.5, which is only slightly lower compared with the results provided in Table 6.

Few results are published in open literature dealing with autothermal reformers in the kW-range. Roychoudhury et al. [23] report of a reactor, which was designed for 3.4 kW_{el} power output. The active layer of the reactor was composed of metal meshes coated with Rh-CeZr catalyst. Ninety-seven percent conversions were achieved only for O/C ratios exceeding 0.9. At S/C 1.5 and O/C 1.0, the hot spot temperature amounted to 732 °C. 33.6% H_2, 43.7% N_2, 0.3% CH_4, 8.2% CO and 14.1% CO_2 were found in the reformate on dry basis. Higher content of hydrogen could be gained at S/C 1.2 and O/C 0.63; however, conversion was only 68%. Despite the lower conversion achieved by Roychoudhury et al., the dry reformate composition was similar compared with the numbers provided in Table 6: 39.7% H_2, 39.8% N_2, 0.12% CH_4, 7.3% CO and 15.4% CO_2 were found in the reformate. The methane content of the reformate was considerably lower compared to the values reported in the current paper.

7. Outlook

After the experimental verification of the functionality of the reactor, it was then removed from the test rig and incorporated into a complete fuel processor (including CO-clean-up reactors). Results from the operation of this fuel processor will be reported in a separate follow-up paper.

Acknowledgement

The authors gratefully acknowledge the financial support of this work by the European Commission in the scope of the project MINIREF contract-no: ENK6-CT-2001-00515.

References

[1] G. Kolb, V. Hessel, Review: micro-structured reactors for gas phase reactions, Chem. Eng. J. 98 (2004) 1.
[2] V. Hessel, H. Löwe, A. Müller, G. Kolb, 2005, Chemical Micro Process Engineering, vol. 2, Processing, Applications and Plants, Chapter 2, Microstructured fuel processors for energy generation, Wiley, Weinheim, ISBN-13 978-3-527-30998-6, p. 281 ff.
[3] J.-M. Bae, S. Ahmet, R. Kumar, E. Doss, J. Power Sources 139 (2005) 91–95.

[4] E.R. Delsman, B.J.P.F. Laarhoven, M.H.J.M. de Croon, G.J. Kramer, J.C. Schouten, Chem. Eng. Res. Des. 83 (2005) 1063–1075.
[5] H.-S. Hwang, R.M. Yarrington, R.M. Heck, United States Patent 4522894 (1985).
[6] S.H. Chan, H.M. Wang, J. Power Sources 101 (2001) 188–195.
[7] J.N. Armor, Appl. Catal. A: Gen. 176 (1999) 159–176.
[8] C. Palm, P. Cremer, R. Peters, D. Stolten, J. Power Sources 106 (2002) 231–237.
[9] M.E.S. Hegarty, A.M. O'Connor, J.R.H. Ross, Catal. Today 42 (1998) 225–232.
[10] V.R. Choudhary, S. Banerjee, A.M. Rajput, Appl. Catal. A: Gen. 234 (2002) 259–270.
[11] B. Lindström, J. Agrell, L.J. Pettersson, Chem. Eng. J. 93 (2003) 91–101.
[12] K. Nagaoka, K. Seshan, K. Aika, J.A. Lercher, J. Catal. 197 (2001) 34–42.
[13] K. Nagaoka, M. Okamura, K. Aika, Catal. Comm. 2 (2001) 255–260.
[14] L.L.G. Jacobs, P.W. Lednor, A.G.G. Limahelu, R.J. Schoonebeek, K.A. Vonkeman, United States Patent 5,510,056, Assignee: Shell Oil Company (Houston, TX) April 23, 1996.
[15] R.M. Heck, P. Flanagan, United States Patent 4,844,837, Assignee: Engelhard Corporation (Menlo Park, NJ), July 4, 1989.
[16] K. Heitnes Hofstad, J.H.B.J. Hoebink, A. Holmen, G.B. Marin, Catal. Today 40 (1998) 157–170.
[17] A. Qi, S. Wang, G. Fu, D. Wu, Appl. Catal. A: Gen. 293 (2005) 71–82.
[18] B.E. Yoldas, J. Mater. Sci. 10 (1975) 1856.
[19] H. Katz, P. Alphonse, M. Courty, French Patent no. 04.50105 (2004).
[20] H. Ehwald, U. Leibnitz, H. Lieske, Catal. Lett. 70 (2000) 23–26.
[21] H. Ehwald, D.L. Hoang, U. Leibnitz, H. Lieske, Stud. Surf. Sci. Catal. 139 (2001) 117–124.
[22] C. Severin, S. Pischinger, J. Ogrzewalla, J. Power Sources 145 (2005) 675–682.
[23] S. Roychoudhury, M. Castaldi, M. Lyobowski, R. LaPierre, S. Ahmed, J. Power Sources 152 (2005) 75–86.